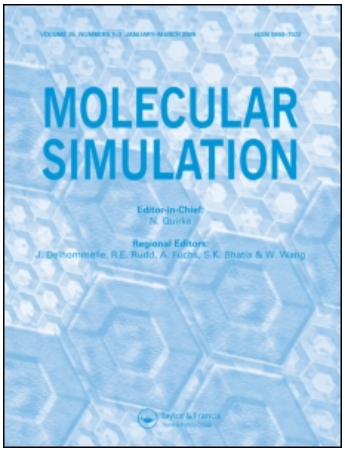

Molecular Simulation
Publication details, including instructions for authors and subscription information:
http://www.informaworld.com/smpp/title~content=t713644482

Calcium hydration on montmorillonite clay surfaces studied by Monte Carlo simulation

Jeffery A. Greathouse[a]; Erik W. Storm[a]
[a] Department of Chemistry, St. Lawrence University, Canton, NY, USA

Online publication date: 26 October 2010

To cite this Article Greathouse, Jeffery A. and Storm, Erik W.(2002) 'Calcium hydration on montmorillonite clay surfaces studied by Monte Carlo simulation', Molecular Simulation, 28: 6, 633 — 647
To link to this Article: DOI: 10.1080/0892702029003
URL: http://dx.doi.org/10.1080/0892702029003

Molecular Simulation, 2002 VOL. 28 (6-7), pp. 633–647

CALCIUM HYDRATION ON MONTMORILLONITE CLAY SURFACES STUDIED BY MONTE CARLO SIMULATION

JEFFERY A. GREATHOUSE* and ERIK W. STORM

Department of Chemistry, St. Lawrence University, Canton, NY 13617, USA

(Received 1 April 2001; In final form 1 August 2001)

Monte Carlo computer simulations were used to investigate the interlayer structure of Ca-montmorillonite for hydration levels ranging from the dry clay to a three-layer system. Our model of montmorillonite consists of negative charge sites in both the octahedral and tetrahedral layers. Our results are compared with X-ray diffraction data from Ca-clays, which have suggested an interlayer structure similar to Mg-clays. However, the Ca^{2+} co-ordination number in these systems and in bulk liquid is a subject of ongoing debate. Our results support an eightfold water solvation shell for calcium, even within the confines of a clay pore. The Ca^{2+} co-ordination number decreased at lower water content, as the water layer became constrained and less like bulk liquid. Additionally, Ca^{2+} solvation shells included surface oxygen atoms at low water content, although this may be a result of the Ca–O interaction potentials.

Keywords: Monte Carlo simulation; Clay; Calcium; Solvation; Co-ordination number

INTRODUCTION

Determination of the solvation structure of aqueous calcium ions is a challenging spectroscopic task due to water exchange within the first hydration shell and the low atomic weights of atoms in this system. However, an understanding of the structure of calcium in aqueous clay systems is essential because Ca-smectites constitute a great portion of soils, sedimentary rocks, and biological systems. The issue of Ca^{2+} hydration is further complicated upon examination of crystal

*Corresponding author. E-mail: jgreathouse@stlawu.edu.

ISSN 0892-7022 © 2002 Taylor & Francis Ltd
DOI: 10.1080/08927020290030170

structures of calcium-containing proteins, in which oxygen was the chief liganding atom. Katz *et al*.examined 309 such structures and concluded that Ca^{2+} co-ordination numbers of 6, 7, and 8 are common [1]. The geometry and energetics of Ca^{2+} hydration in vacuum have been studied by *ab initio* quantum mechanical calculations. The clusters $Ca(H_2O)_4^{2+}$ and $Ca(H_2O)_5^{2+}$ were considerably higher in energy than $Ca(H_2O)_6^{2+}$, while no significant energy difference was found for hydration numbers of 6, 7 or 8 [1].

Several simulation studies have been carried out to investigate calcium hydration in bulk water. Obst *et al*. [2] used the TIP3P [3] water model and CHARMM [4] parameters for Ca^{2+}, and a first-shell co-ordination number (CN) of 8.0 was obtained. The solvation shell was also found to be long-lived, with half of the initial solvating waters still in the solvation shell after 1 ns of simulation time. More recently, a series of classical molecular dynamics (MD) simulations were performed for aqueous Ca^{2+} in tandem with *ab initio* MD for the solvation shell. Using a purely classical forcefield, the CN was 9.2, which decreased to a value of 8.3 with the *ab initio* method [5]. For constant volume MD simulations using the SPC/E water model, ion–water parameters taken from the Gromos program [6], Aquist [7], and Dang and Smith [8] resulted in Ca^{2+} co-ordination numbers of 8.0, 7.4, and 7.9, respectively [9]. A recent comparison of MD simulations was made with X-ray scattering data for $CaCl_2$ solutions [10]. MD results using the GROMOS Ca^{2+}–water potential [6] showed a CN of 8.0, which agreed well with experiment. MD results using the Aquist [7] and Bounds [11] parameters for Ca^{2+}–water gave co-ordination numbers of 7.9 and 9.5, respectively. Polarization and nonadditivity effects have been included in Monte Carlo simulations of aqueous Mg^{2+} and Ca^{2+} using the MCHO potential form [12]. Ion–water radial distribution functions showed a well-defined depletion layer for Mg^{2+}, indicating that exchange of water molecules between the first and second hydration shells does not readily occur. The corresponding depletion zone for Ca^{2+} was not as well defined, indicating that the first hydration shell of Ca^{2+} is not static. The results to date indicate that the Ca^{2+} hydration structure in bulk solution is highly dependent on the potential parameters used for ion–water interactions.

The structure of aqueous ions adsorbed to clay mineral surfaces has been the topic of experimental and theoretical research [13]. Smectites are charged 2:1 clay minerals with $Al(OH)_6^{3-}$ octahedra sandwiched between silica tetrahedra [14]. Negative surface charge arises naturally in these systems due to isomorphic substitution in the octahedral layer, tetrahedral layer, or both. When immersed in aqueous electrolyte solution, the smectite charge is balanced by hydrated cations in the interlayer region. The charged clay plates are thus separated by thin regions of aqueous solution, and the $d(001)$ spacing between plates is measured by X-ray

diffraction. The vermiculite clay is characterized by substitution of Al^{3+} for Si^{4+} in the tetrahedral layer only, resulting in high surface charges of approximately 1.5 *e* per unit cell [14]. Using Ca^{2+} as the charge-balancing interlayer cation, the *d*(001) spacings have been measured at 14.97 and 15.05 Å, corresponding to the two-layer hydrate [15,16]. Smectite clays result from charge substitution in both the octahedral or tetrahedral layers and possess a lower surface charge of 0.75 *e* per unit cell. Recently Tamura *et al*. [17] measured the *d*(001) spacing of calcium-exchanged synthetic montmorillonite and found values of 11.9, 15.2, and 18.1 Å for the one-, two-, and three-layer hydrates, respectively. This value for the two-layer hydrate is consistent with studies of naturally occurring Ca-vermiculite [15,16]. Also seen were smaller peaks in between the 2- and 3-layer hydrates, which were attributed to a random mixture of hydration states. The authors found that only synthetic smectite displayed the stepwise decrease in layer spacing, while diffraction studies performed on a natural smectite showed a continuous hydration/dehydration. Although the layer spacing is static on the X-ray diffraction time scale, the Ca^{2+} co-ordination number in these otherwise well-defined systems has been assigned values of either six or eight [15,16]. Monte Carlo and molecular dynamics simulation studies on aqueous clay systems serve as a useful guide in the interpretation of experimental data. In addition to providing averaged thermodynamic results for comparison to available experimental data, the structure and dynamics of the clay interlayer region may be visualized through snapshots. Simulation studies of aqueous clays have been performed with both monovalent and divalent interlayer cations under constraints of constant pressure [18–21], volume [22–24], and chemical potential [25–27]. The goal of this work was to investigate the hydration structure of Ca^{2+} ions near montmorillonite clay surfaces using Monte Carlo simulation. Specifically, we have examined the equilibrium hydration structure of interlayer Ca^{2+} ions as the number of interlayer water molecules is varied. To our knowledge, these are the first reported simulations of Ca^{2+} hydration structure near charged clay mineral surfaces.

METHODS

Monte Carlo simulations were performed with the code Monte [28], and all molecules were treated as rigid bodies. We used the model of Skipper *et al*. [20] for the montmorillonite clay lattice, so only a brief description will be provided here. A simulation supercell containing approximately eight unit cells of the clay was constructed, resulting in a patch with dimensions 21.12 × 18.28 Å in the (x, y) plane. Co-ordinates for clay atoms were taken from X-ray diffraction data

for talc [29]. The layer spacing, as determined by the z-axis of the simulation supercell and analogous to the experimental $d(001)$ spacing, was assigned an initial value of 17.0 Å for all runs. Negative charge sites in the clay lattice were created by substituting Al for Si in the tetrahedral layer or Mg for Al in the octahedral layer with a corresponding reduction of one elementary charge (e) in each case. Four octahedral and two tetrahedral charge sites were distributed randomly throughout the lattice, which were balanced by three interlayer Ca^{2+} ions. The resulting unit cell formula for Ca-montmorillonite was obtained:

$$Ca_{0.375}[Si_{7.75}Al_{0.25}](Al_{3.5}Mg_{0.5})O_{20}(OH)_4$$

where [ ] refers to atoms in the tetrahedral layer and ( ) refers to atoms in the octahedral layer. Structural hydroxyl groups were directed toward vacancies in the octahedral layer. Partial atomic charges and van der Waals parameters for clay oxygen atoms and interlayer water molecules were taken from the TIP4P water model [3]. Parameters for Ca–O van der Waals interactions (ion–water and ion–clay) were taken from Aquist [7]. Simulations of Ca^{2+} ions in aqueous solution using the Aquist potential show a CN of 8 and an average Ca–O distance of 2.46 Å in the first hydration shell, in agreement with X-ray spectroscopic and scattering experiments of aqueous calcium chloride solutions [10]. The relative merits of currently available Ca–O potentials is a subject of ongoing research [1,2,9,10], but the Aquist potential appears to be suited for aqueous environments such as those encountered in our simulations. The interaction potential energy U was calculated using the Lennard–Jones format (in kJ mol^{-1}):

$$U = \sum_i \sum_j \frac{q_i q_j}{4\pi\varepsilon_0 r_{ij}^2} + \frac{A_i A_j}{r_{ij}^{12}} - \frac{B_i B_j}{r_{ij}^6} \tag{1}$$

TABLE I Potential parameters for interlayer species (distances in Å, partial charges in e, and interaction energies in kJ mol^{-1})

Layer	Atom type	q	A	B
Interlayer	Ca	2.00	540.2	38.50
	O	−1.04	1584	50.52
	H	0.52	0.0	0.0
Tetrahedral	O	−1.04	1584	50.52
	Si	1.20	0.0	0.0
	Al	0.20	0.0	0.0
Apical	O	−1.00	1584	50.52
Octahedral	O	−1.52	1584	50.52
	H	0.52	0.0	0.0
	Al	3.00	0.0	0.0
	Mg	2.00	0.0	0.0

where q_i represents the partial charge for atom i, r_{ij} is the separation (in Å) between atoms i and j, and the A_i and B_i represent the van der Waals parameters. All parameters are given in Table I. Simulations were performed under the constraints of constant temperature ($T = 300$ K) and pressure applied to the clay layers ($\sigma = 100$ kPa).

Our simulation methodology is based on previous studies of aqueous ion–clay interactions [20–23,30,31]. Initial interlayer configurations were generated by

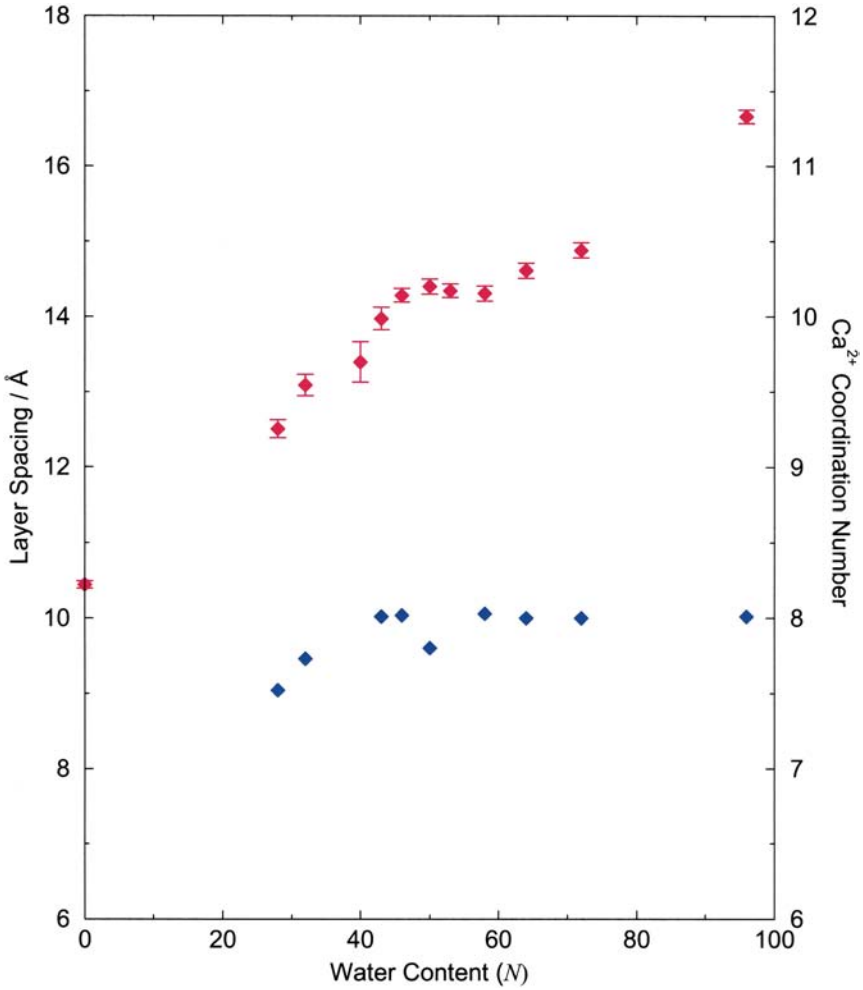

FIGURE 1 Averaged layer spacing (red symbols) and Ca^{2+} co-ordination number (blue symbols) versus water content for $N = 0$ through $N = 96$. Standard deviations in the layer spacing are indicated by bars at each water content.

placing Ca^{2+} ions at the midplane directly above (or below) a surface charge site. A total of *N*water molecules were then placed randomly throughout the interlayer region, and periodic boundary conditions were used to replicate the simulation supercell infinitely in three dimensions. For reference, $N = 32$ corresponds to a water content of 0.1 g H_2O/g clay [32]. Short-range interactions were treated in the all-image convention with a cutoff of 9.0 Å, and electrostatic interactions were computed using the Ewald sum method with a cutoff of 3.0 $Å^{-1}$. Equilibration was established by first allowing movement of water molecules only for 50,000 steps, followed by movement water and the upper clay layer in the *z*-direction only for an additional 50,000 steps. After a third segment of 50,000 steps (water molecules and the upper clay layer in any direction), all species, including interlayer Ca^{2+} ions, were allowed full motion. Throughout the simulations, a movement by the upper clay layer was attempted for every five complete cycles of interlayer movements [20]. Equilibrium was established by monitoring the layer spacing and total potential energy, *U*. The simulations were continued for at least an additional 500,000 steps once equilibrium was established.

RESULTS AND DISCUSSION

Fig. 1 shows averaged layer spacing and Ca^{2+} co-ordination numbers as a function of interlayer water content for Ca-montmorillonite. At lower water contents ($N = 28–40$) corresponding to the one-layer hydrate, the layer spacing increases as water is added to the system. As the water content increases, a plateau in the layer spacing is reached at approximately 14.3 Å. A likely explanation for this behavior may be found by examining the corresponding Ca^{2+} CN, which reaches its maximum value of 8.0 at $N = 43$. Empty space in the interlayer region is then occupied by additional water molecules up to $N = 58$. Beyond this value, additional water molecules may be accommodated only by an increase in the layer spacing. This behavior suggests the formation of metastable states between the one- and two-layer hydrates, as seen in X-ray diffraction experiments [17] and also in simulations of Sr-montmorillonite [19]. The two-layer hydrate showed an experimental layer spacing of 15.2 Å, which is significantly larger than our plateau value of 14.3 Å. However, experimental layer spacings for the random mixture of one- and two-layer hydrates ranged from approximately 14.5–15.0 Å [17]. Previous simulations of Mg-beidellite resulted in a calculated layer spacing for the two-layer hydrate that was also lower than the experimental value [21]. This suggests that discrepancies in simulated and experimental layer spacing values may be due to the smectite

model used in these studies. Additionally, because the unit cell formula of the synthetic clay was not reported by Tamura *et al*. [17], it is likely that the number and location of charge sites (tetrahedral layer or octahedral layer) are different from our model. Given this difference, our calculated layer spacing for the two-layer hydrate provides an acceptable comparison with available experimental data. Our calculated layer spacing for the dehydated clay is 10.4 Å (Fig. 1). While a corresponding value was not reported for Ca-montmorillonite [17], an experimental value of 9.50 Å was reported for dehydrated Ca-vermiculite [33]. Due to the differences in these model systems cited previously, we maintain that the validity of the Aquist Ca–O potential cannot be judged solely on a comparison of layer spacings for dehydrated clays.

A Ca^{2+} CN of 8.0 was the expected result for systems with a high water content since this is the value for Ca^{2+} ions in bulk water given by the Aquist parameters [9,10]. Calcium ions in lower water content systems had, as expected, lower coordination numbers due to the confines of a smaller system with fewer water

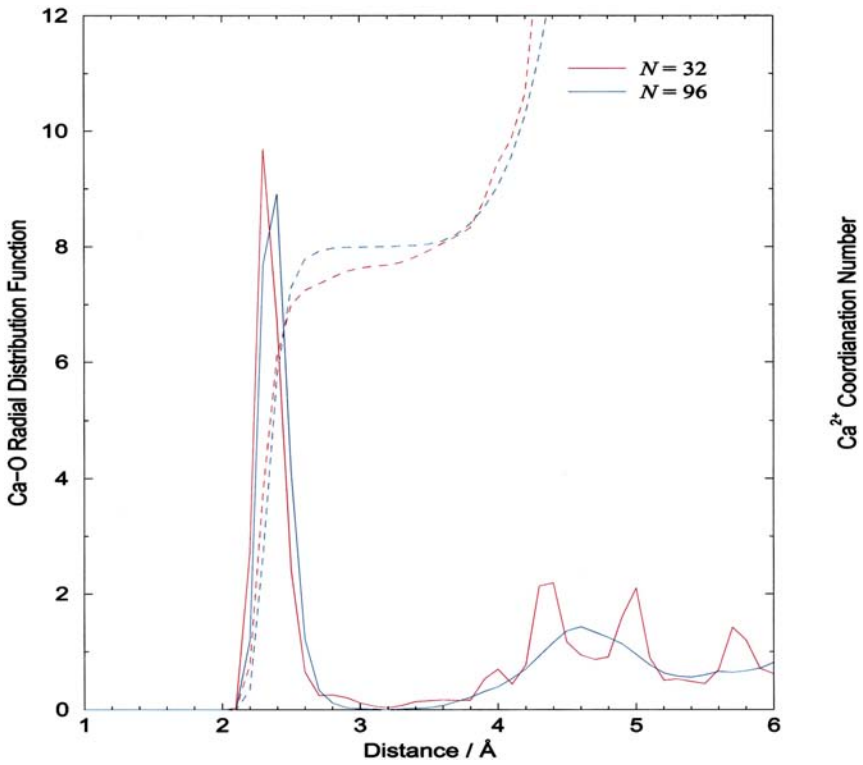

FIGURE 2 Averaged Ca–O radial distribution functions (solid lines) and running Ca^{2+} coordination number (dashed lines) for $N = 32$ and $N = 96$.

molecules. One or more Ca^{2+} ions moved to the surface and became solvated by surface oxygens, which resulted in a compression of the layer spacing. There is little experimental data to verify this interlayer structure, however recent IR spectroscopic experiments of Ca-montmorillonite show pronounced changes in H_2O vibrational frequencies when the water content is at or below 15 H_2O molecules/Ca^{2+} ion [34]. According to Fig. 1, the upper-limit for the one-layer hydrate is $N = 40$, or approximately 13 H_2O molecules/Ca^{2+} ion. As water is removed in the IR desorption experiments, the transition from a two-layer to a one-layer hydrate may result in the observed H_2O vibrational shifts. A comparison with H_2O vibrational spectra is best accomplished with molecular dynamics simulations, which is an area of current research.

Details of the Ca^{2+} hydration structure emerge from analysis of averaged Ca–O radial distribution function (RDF) data. RDFs were calculated by averaging the number of atomic species within radial shells about the central atom [20]. For Ca–O pairs, clay oxygen atoms were included since these atoms constitute a portion of the ion hydration shell of inner-sphere surface complexes [14]. Calcium co-ordination numbers were determined by integrating the first peak in the Ca–O RDF, using the first minimum in the curve as the upper limit of integration. Two such RDF graphs ($N = 32$ and $N = 96$) are shown in Fig. 2 along with the running Ca^{2+} CN, and data from the first Ca–O peak are summarized in Table II. Bin widths were assigned a value 0.1 Å in the simulations, so the Ca–O distances at the first maximum (d_{max}) and first minimum (d_{min}) are given to the nearest 0.05 Å. Because clay oxygen atoms were included in the RDF binning process, only slight differences exist between co-ordination numbers of fully hydrated and partially dehydrated Ca^{2+} ions. At lower water content, Ca^{2+} ions are more likely to form inner-sphere surface

TABLE II Ca–O distances at first maximum (d_{max}) and first minimum (d_{min}), and Ca^{2+} co-ordination number (CN) at first minimum

N	d_{max} (Å)	d_{min} (Å)	CN
28	2.30	3.25	7.5
32	2.30	3.20	7.7
40	2.35	2.90	7.7
43	2.35	3.00	8.0
46	2.35	3.30	8.0
50	2.35	3.20	7.8
53	2.35	3.30	8.0
58	2.35	3.20	8.0
64	2.40	3.30	8.0
72	2.40	3.30	8.0
96	2.40	3.20	8.0

complexes, and the presence of surface oxygen atoms has a dramatic effect on the second Ca–O peak for $N = 32$ (Fig. 2). The average Ca–O distance is slightly smaller when surface oxygen atoms replace water oxygen atoms in the solvation shell, resulting in a lower value of d_{max}. The metastable region between the one- and two-layer hydrates (see Fig. 1) produces inconsistencies in the RDF data for $N = 40$ through $N = 58$. Specifically, values for d_{min} range from 2.90 to 3.30 Å, indicating that the Ca^{2+} hydration shell includes surface oxygen atoms. Surprisingly, the Ca^{2+} co-ordination number reaches its plateau value of 8.0 in this metastable region, except for the value of 7.8 at $N = 50$.

An equilibrium snapshot (x–z plane) of the 32-water system is shown in Fig. 3 and is characterized by a single layer of interlayer water with Ca^{2+} ions above or below the midplane. The two water molecules well above (and below) the midplane are tucked into ditrigonal cavities on the clay surface. This water adsorption phenomena has been seen previously in clay simulations studies with both monovalent and divalent interlayer ions [21,23,25]. The average Ca^{2+} CN from this simulation is 7.7, which includes both water oxygen atoms and surface oxygen atoms. Approximately half of the interlayer water molecules solvate Ca^{2+} ions, with the remaining solvating oxygen atoms coming from the clay surface. Thus, few water molecules are left to occupy gaps between hydrated ions. The two Ca^{2+} ions located well above and below the midplane have formed inner-sphere complexes near tetrahedral charge sites, and the three adjacent surface oxygen atoms are included in the first hydration shell. The simulation supercell (dashed lines) forms a parallelogram as opposed to the initial rectangular configuration. Average x- and y-co-ordinates for the upper clay layer are

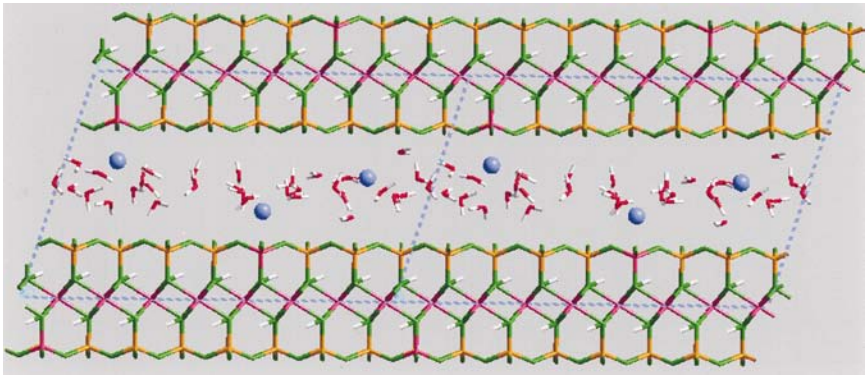

FIGURE 3 Equilibrium snapshot (x, z plane) for $N = 32$. All species are shown as cylinders except for Ca^{2+} ions, which are shown as spheres. The color scheme is as follows: clay O (green), Si (orange), Al or Mg (pink), Ca (blue), interlayer water O (red), H (white). The simulation supercell is repeated in the x-direction, and supercell boundaries are represented by dashed lines.

4.16 ± 0.16 and 0.33 ± 0.19 Å, compared to initial values of 0.0 for each. These results indicate that the upper clay layer has undergone a significant registration process in order to maximize interactions between Ca^{2+} ions and octahedral charge sites. Experimental data on this system are not available for comparison, but Ca^{2+} ions are thought to be fully solvated by interlayer water (i.e. outer-sphere surface complexes) at higher water contents. The equilibrium solvation structure shown here with inner-sphere surface complexes may be a result of the Aquist potential parameters for Ca^{2+}–water interactions. This water content ($N = 32$) has been established as the 1-layer hydrate for other aqueous clay systems [30], and monolayer coverage is indeed verified by this snapshot and averaged oxygen density profiles (data not shown). Additionally, the hydrogen bonding network between water molecules is disrupted because each interlayer molecule is accessible to hydrogen bonds with either clay surface. At low water contents, the decrease in water–water hydrogen bonding is the likely explanation for the decrease in the H–O–H bending frequency and increase in O-H stretching frequency seen in IR experiments [34].

As the water content is doubled to $N = 64$, two well-defined water layers develop, as seen in Fig. 4. Additionally, Ca^{2+} ions are fully hydrated and have taken up positions in the midplane, in agreement with experiment [15,16]. Each Ca^{2+} ion is surrounded by eight solvating waters that reside above and below the midplane, resulting in a square antiprism solvation geometry. These hydration shells provide a barrier so that nonsolvating water molecules are excluded from the midplane. Average *x*- and *y*-co-ordinates for the upper clay layer are −1.60 ± 0.33 and 2.08 ± 0.59 Å, and the larger average deviations indicate that

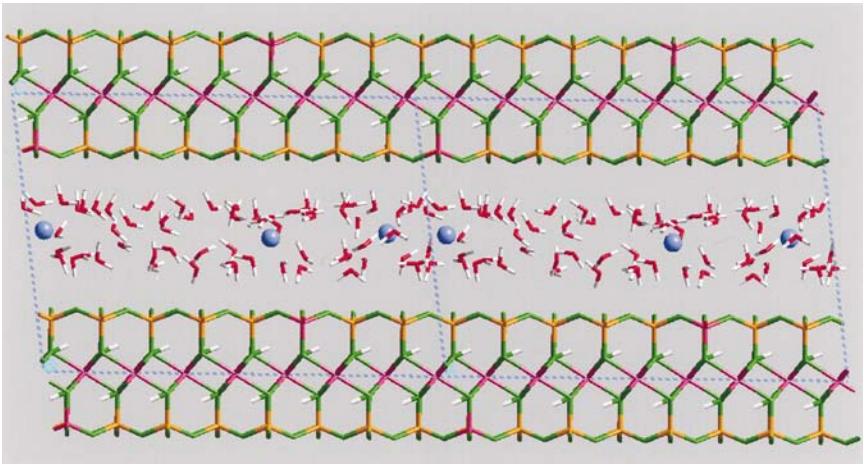

FIGURE 4 Equilibrium snapshot (*x*, *z* plane) for $N = 64$ with all designations as in Fig. 3.

no energy-minimized clay registration exists. Ion–clay interactions are now screened by a full monolayer of water molecules above and below the midplane, so clay registration may not be as important for equilibration compared to the $N = 32$ systems. In this snapshot we also see no evidence of water adsorption into ditrigonal cavities, unlike the lower hydrates. At this water content it is energetically more favorable for water molecules to form a hydrogen bonded network than for a percentage to be adsorbed to the surface. The tendency of nonsolvating water molecules to occupy ditrigonal cavities is influenced by the clay hydroxide orientation [23] and water content [25].

The antiprism Ca^{2+} hydration shell that is common for water contents of $N = 48$ and above is shown in Fig. 5 for the $N = 96$ system. Solvating water molecules constitute only 25% of the total water content, and from Fig. 1 we see that the layer spacing has increased well beyond the two-layer hydrate plateau. This system is termed the three-layer hydrate through rational extension of the

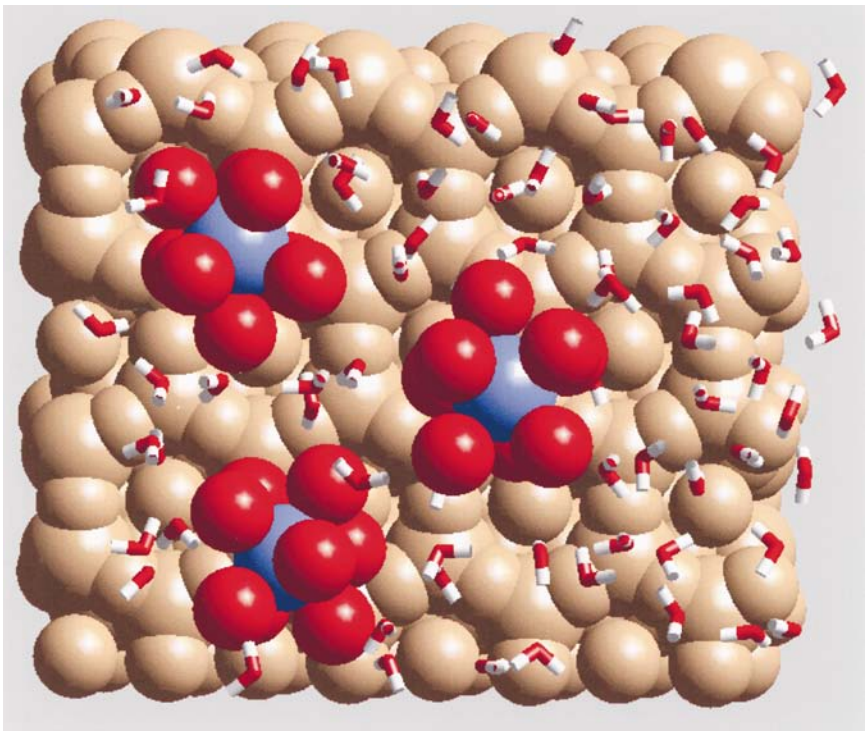

FIGURE 5 Equilibrium snapshot (x, y plane) for $N = 96$, showing one supercell. All species are shown as spheres except for nonsolvating water molecules, which are shown as cylinders. Atoms in the clay layer are colored tan, and interlayer Ca and water molecules are colored as in Fig. 2. Hydrogen atoms on solvating water molecules have been removed for clarity.

chosen values for the one and two layer systems, but we see no evidence of a plateau in the layer spacing values at this water content (Fig. 1). Water molecules and Ca^{2+} ions coexist in the midplane region, allowing for rotational freedom of the $Ca(H_2O)_8^{2+}$ hydration complexes. Specifically, the $Ca(H_2O)_8^{2+}$ complex in the lower portion of Fig. 5 is slightly skewed, which supports the previous statement. In the two-layer hydrate, solvating water molecules are oriented to maximize hydrogen bonding with surface oxygen atoms, causing the exclusion of water molecules at the midplane. For $N = 96$, however, solvating waters are equally likely to form hydrogen bonds with neighboring water molecules or surface oxygen atoms. The location of $Ca(H_2O)_8^{2+}$ hydration complexes in the (x,y) plane is still controlled by charge sites in the clay lattice, however. Nonsolvating water molecules have now occupied all available interlayer space, and we predict that beyond this point the layer spacing will increase linearly with additional water.

CONCLUSION

We have performed Monte Carlo simulations of aqueous Ca-montmorillonite for a range water contents. Both Ca^{2+} CN and layer spacing are greatly affected by the type of Ca^{2+} surface complex formed. At low water contents, Ca^{2+} ions form inner-sphere surface complexes near tetrahedral charge sites, with clay oxygen atoms taking up positions in the first hydration shell. This structure results in reduced values for both Ca^{2+} CN and layer spacing. Both the Ca^{2+} CN and the clay layer spacing increase with increasing water content, but a plateau in the layer spacing for the two-layer hydrate identifies a metastable swelling state. This metastable region is characterized by erratic behavior in Ca^{2+} hydration, as noted by the first minima in the Ca–O RDF. At higher water contents ($N > 64$) only outer-sphere surface complexes are seen. The Ca^{2+} hydration shell consists of eight water molecules in a square antiprism geometry, which is consistent with Aquist parameters for Ca^{2+} in bulk water. These $Ca(H_2O)^{2+}$ complexes serve to keep the clay layer apart even as gaps in the midplane still exist. Additional water molecules fill in the empty spaces at the midplane, and eventually water molecules may be added only with an increase in layer spacing.

Acknowledgements

This research was supported by St. Lawrence University and a Stradling Summer Research Fellowship (E.W.S.). Thanks to Keith Refson and Cliff Johnston for helpful discussions.

References

[1] Katz, A.K., Glusker, J.P., Beebe, S.A. and Bock, C.W. (1996) "Calcium ion co-ordination: a comparison with that of beryllium, magnesium, and zinc", *J. Am. Chem. Soc.* **118**, 5752.

[2] Obst, S. and Bradaczek, H. (1996) "Molecular dynamics study of the structure and dynamics of the hydration shell of alkaline and alkaline-earth metal cations", *J. Phys. Chem.* **100**, 15677.

[3] Jorgensen, W.L., Chandrasekhar, J., Madura, J.D., Impey, R.W. and Klein, M.L. (1983) "Comparison of simple potential functions for simulating liquid water", *J. Chem. Phys.* **79**, 926.

[4] Brooks, B.R., Bruccoleri, R.E., Olafson, B.D., States, D.J., Swaminathan, S. and Karplus, M. (1983) "CHARMM: a program for macromolecular energy, minimization, and dynamics calculations", *J. Comp. Chem.* **4**, 187.

[5] Tongraar, A., Liedl, K.R. and Rode, B.M. (1997) "Solvation of Ca^{2+} in water studied by born-oppenheimer *ab initio* QM/MM dynamics", *J. Phys. Chem. A* **101**, 6299.

[6] van Gunsteren, W.F. and Berendsen, H.J.C. (1987) GROningen MOlecular Simulation (GROMOS) package, Biomos n.v. Ninborgh 16, 4767 AG Groningen, The Netherlands.

[7] Aquist, J. (1990) "Ion–water interaction potentials derived from free energy perturbation simulations", *J. Phys. Chem.* **94**, 8021.

[8] Dang, L.X. and Smith, D.E. (1995) "Comment on "Mean force potential for the calcium-chloride ion pair in water" [J. Chem. Phys. 99, 4229 (1993)]", *J. Chem. Phys.* **102**, 3483.

[9] Guardia, E., Sese, G., Padro, J.A. and Kaklo, S.G. (1999) "Molecular dynamics simulation of Mg^{2+} and Ca^{2+} ions in water", *J. Soln. Chem.* **28**, 1113.

[10] Jalilehvand, F., Spangberg, D., Lindquist-Reis, P., Hermansson, K., Persson, I. and Sandstrom, M. (2001) "Hydration of the calcium ion: an EXAFS, large-angle X-ray scattering, and molecular dynamics simulation study", *J. Am. Chem. Soc.* **123**, 431.

[11] Bounds, D.G. and molecular, A. (1985) "dynamics study of the structure of water around the ions Li^+, Na^+, K^+, Ca^{++}, Ni^{++}, and Cl^-", *Mol. Phys.* **54**, 1335.

[12] Bernal-Uruchurtu, M.I. and Ortega-Blake, I. (1995) "Refined Monte Carlo study of Mg^{2+} and Ca^{2+} hydration", *J. Chem. Phys.* **103**, 1588.

[13] Sposito, G., Skipper, N.T., Sutton, R., Park, S.-H., Soper, A.K. and Greathouse, J.A. (1999) "Surface geochemistry of the clay minerals", *Proc. Natl. Acad. Sci. USA* **96**, 3358.

[14] Sposito, G. (1984) The Surface Chemistry of Soils (Oxford University Press, New York).

[15] Skipper, N.T., Soper, A.K. and Smalley, M.V. (1994) "Neutron diffraction study of calcium vermiculite: hydration of calcium ions in a confined environment", *J. Phys. Chem.* **98**, 942.

[16] Slade, P.G., Stone, P.A. and Radoslovich, E.W. (1985) "Interlayer structures of the two-layer hydrates of Na- and Ca-vermiculites", *Clays Clay. Miner.* **33**, 51.

[17] Tamura, K., Yamada, H. and Nakazawa, H. (2000) "Stepwise hydration of high-quality synthetic smectite with various cations", *Clays Clay Miner.* **48**, 400.

[18] Boek, E.S. and Coveney, P.V. (1995) "Molecular modeling of clay hydration: a study of hysteresis loops in the swelling curves of sodium montmorillonites", *Langmuir* **11**, 4629.

[19] Young, D.A. and Smith, D.E. (2000) "Simulations of clay mineral swelling and hydration: dependence upon interlayer ion size and charge", *J. Phys. Chem. B* **104**, 9163.

[20] Skipper, N.T., Chang, F.-R.C. and Sposito, G. (1995) "Monte Carlo simulation of interlayer molecular structure in swelling clay minerals—1: methodology", *Clays Clay Miner.* **43**, 285.

[21] Greathouse, J.A., Refson, K. and Sposito, G. (2000) "Molecular dynamics simulation of water mobility in magnesium-smectite hydrates", *J. Am. Chem. Soc.* **122**, 11459.

[22] Chang, F.-R.C., Skipper, N.T. and Sposito, G. (1995) "Computer simulation of interlayer molecular structure in sodium montmorillonite hydrates", *Langmuir* **11**, 2734.

[23] Greathouse, J.A. and Sposito, G. (1998) "Monte Carlo and molecular dynamic simulations of interlayer structure in $Li(H_2O)_3$-smectites", *J. Phys. Chem. B.* **102**, 2406.

[24] Titiloye, J.O. and Skipper, N.T. (2000) "Computer simulation of the structure and dynamics of methane in hydrated Na-smectite clay", *Chem. Phys. Lett.* **329**, 23.

[25] Karaborni, S., Smit, B., Heidug, W., Urai, J. and van Oort, E. (1996) "The swelling of clays: molecular simulations of the hydration of montmorillonite", *Science* **271**, 1102.

[26] Shroll, R.M. and Smith, D.E. (1999) "Molecular dynamics simulations in the grand canonical ensemble: application to clay mineral swelling", *J. Chem. Phys.* **111**, 9025.

[27] Chavez-Paez, M., Van Workum, K., de Pablo, L. and de Pablo, J.J. (2001) "Monte Carlo simulations of Wyoming sodium montmorillonite hydrates", *J. Chem. Phys.* **114**, 1405.

[28] Skipper, N.T. (1996) MONTE User's Manual (Department of Physics and Astronomy, University College, London).
[29] Brindley, G.W. and Brown, G. (1980) Crystal Structures of Clay Minerals and Their X-Ray Identification (Mineralogical Society, London).
[30] Skipper, N.T., Sposito, G. and Chang, F.-R.C. (1995) "Monte Carlo simulation of interlayer molecular structure in swelling clay minerals—2: monolayer hydrates", *Clays Clay. Miner.* **43**, 294.
[31] Chang, F.-R.C., Skipper, N.T., Refson, K., Greathouse, J.A. and Sposito, G. (1999) "Interlayer molecular structure and dynamics in Li-, Na-, and K-montmorillonite–water systems", In: Sparks, D.L. and Grundl, T.J., eds, Mineral–Water Interfacial Reactions, ch. 6 (American Chemical Society, Washington, DC).
[32] Newman, A.C.D. (1987) Chemistry of Clays and Clay Minerals (Wiley, New York).
[33] de la Calle, C. and Suquet, H. (1988) "Vermiculite", In: Bailey, S.W., ed, Reviews in Mineralogy (Mineralogical Society of America, Chelsea, MI) **Vol. 19**, p 482.
[34] Xu, W., Johnston, C.T., Parker, P. and Agnew, S.F. (2000) "Infrared study of water sorption on Na-, Li-, Ca-, and Mg-exchanged (SWy-1 and SAz-1) montmorillonite", *Clays Clay. Miner.* **48**, 120.
[35] Allen, M.P. and Tidesley, D.J. (1987) Computer Simulation of Liquids (Clarendon Press, Oxford).

SPECIAL APPENDIX

Hamiltonian

All simulations were performed under the constraints of constant stress and temperature. The acceptance Hamiltonian between states 1 and 2 given by [28]

$$\Delta H = (U_2 - U_1) + P(V_2 - V_1) - \frac{N_c}{k_B T} \ln\left(\frac{V_2}{V_1}\right) \tag{A1}$$

where U is the potential energy, P is the pressure in the z-direction, V is the volume of the supercell containing N_c molecules, k_B is the Boltzmann constant, and T is the Kelvin temperature. Potential parameters for all interactions are provided above.

Algorithm

The Monte Carlo algorithm used in this work is described elsewhere [35]. Techniques for handling short- and long-range interactions with three-dimensional periodic boundary conditions are discussed above.

Averaging of Simulation Data

Atomic co-ordinates (including the upper clay layer) and potential energy are updated at regular intervals of 500 steps. Atomic density profiles, water dipole

orientation, and radial distribution functions are calculated using neighbor lists [35].

Validation of Simulation

Equilibration was determined by monitoring the layer spacing and potential energy. Standard deviations in layer spacing for each simulation are given in Fig. 1. The Ca^{2+} hydration structure was checked by comparing first-shell peaks and running co-ordination numbers from previous studies [9,10]. Averaged layer spacing values were compared with experimental values [15–17] where appropriate.